

High-resolution neutron capture and transmission measurements, and the stellar neutron-capture cross section of ^{88}Sr

P. E. Koehler,¹ R. R. Winters,² K. H. Guber,³ T. Rauscher,^{4,5} J. A. Harvey,¹ S. Raman,¹ R. R. Spencer,³ J. C. Blackmon,¹ D. C. Larson,¹ D. W. Bardayan,¹ and T. A. Lewis¹

¹*Physics Division, Oak Ridge National Laboratory, Oak Ridge, Tennessee 37831*

²*Department of Physics, Denison University, Granville, Ohio 43023*

³*Computational Physics and Engineering Division, Oak Ridge National Laboratory, Oak Ridge, Tennessee 37831*

⁴*Departement für Physik und Astronomie, Universität Basel, CH-4056 Basel, Switzerland*

⁵*Department of Astronomy and Astrophysics, University of California at Santa Cruz, Santa Cruz, California 95064*

(Received 9 June 2000; published 13 October 2000)

We have made new and improved measurements of the neutron capture and total cross sections for ^{88}Sr at the Oak Ridge Electron Linear Accelerator (ORELA). Improvements over previous measurements include a wider incident neutron energy range, better resolution, the use of metallic rather than carbonate samples, better background subtraction, reduced sensitivity to sample-dependent backgrounds, and better pulse-height weighting functions. Because of its small cross section, the $^{88}\text{Sr}(n, \gamma)$ reaction is an important bottleneck during s -process nucleosynthesis. Hence, an accurate determination of this rate is needed to better constrain the neutron exposure in s -process models and to better understand the recently discovered isotopic anomalies in certain meteorites. We performed an \mathcal{R} -matrix analysis of our capture and transmission data to extract parameters for 101 resonances between 100 eV and 350 keV. In addition, we fitted our transmission data alone to extract parameters for 342 additional resonances between 350 and 950 keV. We used this information to calculate average properties of the $^{88}\text{Sr}+n$ system for comparison to previous work. Although previous data and resonance analyses were much less extensive, they are, in general, in good agreement with our results except that the average radiation widths as well as the p -wave correlation coefficients we determined are significantly smaller, and the s -wave correlation coefficient we determined has opposite sign from that reported in previous work. We used these resonance parameters together with a calculation of the small, but significant direct-capture contribution to determine the astrophysical reaction rate for the $^{88}\text{Sr}(n, \gamma)$ reaction to approximately 3% accuracy across the entire range of temperatures needed by s -process models. Our new rate is in good agreement with the results from a high-precision activation measurement at $kT=25$ keV, but it is approximately 9.5% lower than the rate used in most previous nucleosynthesis calculations in the temperature range ($kT=6-8$ keV), where most of the neutron exposure occurs in current stellar models of the s process. We discuss the possible astrophysical impact of this new, lower rate.

PACS number(s): 26.20.+f, 25.40.Lw, 27.50.+e

I. INTRODUCTION

The $^{88}\text{Sr}(n, \gamma)$ cross section is important to nuclear astrophysics for at least three reasons. (i) ^{88}Sr acts as a bottleneck in s -process nucleosynthesis [1]. The $A \approx 100$ region is complicated, with several different nucleosynthesis processes contributing to the abundances of nuclides in this region. For example, the path of the s process near strontium is depicted in Fig. 1. Although the s -process path is complicated by branchings at the radioisotopes ^{85}Kr and ^{86}Rb , all branches eventually lead through ^{88}Sr . Because of its closed neutron shell, the $^{88}\text{Sr}(n, \gamma)$ reaction rate is very small, so it acts as a bottleneck; hence, it is crucial to know accurately the cross section for the $^{88}\text{Sr}(n, \gamma)$ reaction so that the relative contributions of various processes to the solar system abundances can be disentangled. (ii) It has been shown that a measurement of the Rb/Sr ratio in stars can be used to extract the neutron density during the s process. Current results [2] indicate that the neutron density derived from these data is consistent only when the s process occurs during the interpulse phase in low-mass asymptotic giant branch (AGB) stars. Because the cross sections were not measured to low

enough energies such as to determine accurately the low-temperature reaction rates needed in the models, this conclusion is based mainly on extrapolations of previous neutron-capture measurements. Strontium is the normalization point for these data, and strontium is predominantly ^{88}Sr . Therefore, new measurements of the $^{88}\text{Sr}(n, \gamma)$ cross section are needed at lower neutron energies to provide a more robust test of stellar models. (iii) Nonsolar ratios for isotopes of strontium and other elements have been observed in SiC grains in certain meteorites [3]. Such observations provide the s -process abundance ratios for isotopes of several elements, thereby greatly expanding the number of “effectively s only” calibration points for models of the s process. Calculations indicate that isotopes with small (n, γ) cross sections provide the most sensitive test of s -process models when comparing the model results to the meteorite data. Hence, more precise reaction rates are needed for nuclides such as ^{88}Sr to more fully exploit the opportunity offered by meteorite data for improved understanding of the s process and AGB stars.

There have been three previously reported measurements [1,4,5] of the $^{88}\text{Sr}(n, \gamma)$ cross section from which the reac-

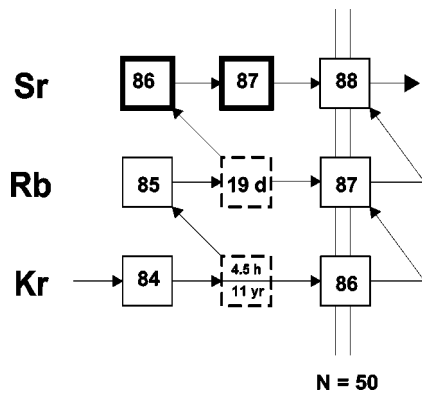


FIG. 1. The s -process path in the strontium region. Arrows depict the path of the s process in this region. Solid boxes represent stable nuclides, and dashed boxes indicate radioactive ones. The thick boxes for ^{86}Sr and ^{87}Sr denote that these two isotopes are produced solely by the s process and, hence, are important calibration points for s -process models. The nucleosynthesis path branches at ^{85}Kr and ^{86}Rb , where neutron capture competes with β decay. However, all branches combine again at ^{88}Sr , which has a closed neutron shell ($N=50$) and, hence, a very small neutron capture cross section.

tion rate has been determined. None of these previous measurements can be used reliably to determine the reaction rate across the range of temperatures needed for stellar model calculations [6]—the first [1] because it was made with a pseudo-Maxwellian source and, hence, determines the reaction rate at the single temperature $kT=25$ keV, and the latter two [4,5] because they are too imprecise and because they did not extend low enough in energy. Also, subsequent work [7] has shown that relatively large systematic errors may plague these data. Finally, a resonance at 2.780 keV has been reported [8], but apparently ignored in evaluations of the reaction rate. Although the reported parameters for this resonance have large uncertainties, inclusion of this resonance leads to a 77% increase in the reaction rate at 5 keV over the rate calculated from all the other resonances reported in Ref. [5]. Hence, it is vitally important to make new measurements in this energy range.

II. EXPERIMENTAL PROCEDURES

The samples were isotopically enriched (99.83% ^{88}Sr , 0.12% ^{87}Sr , and 0.05% ^{86}Sr) metallic strontium. Because strontium metal is chemically very reactive, the samples were fabricated in an inert atmosphere, and the sample for the capture experiment was shipped in a vacuum container. During the experiment, the sample was placed in the evacuated beam line between the γ -ray detectors. The samples for the transmission experiments were sealed in thin-walled, aluminum containers. The use of metallic samples substantially reduced sample-dependent backgrounds and correction factors—as compared to previous measurements in which carbonate samples were used. In addition, the use of metallic rather than carbonate samples in the transmission experiments substantially increased the sensitivity to small resonances.

The measurements were performed using the ORELA white-neutron-source facility. Neutron energy was determined using the time of flight. The capture measurements were made on ORELA flight path 7 at a source-to-sample distance of 40.12 m. The ORELA was operated at a pulse rate of 525 Hz, a pulse width of 8 ns, and a power of 7–8 kW. The sample was 2.54 cm wide by 5.08 cm high by 0.0106 at/b thick. A ^{10}B filter was used to remove overlap neutrons from preceding beam bursts, and a Pb filter was used to reduce γ -flash effects. These filters were placed in the beam at a distance of 5 m from the neutron source. The capture cross sections were determined using the pulse-height weighting technique with a pair of C_6D_6 scintillators, which served as the γ -ray detectors. The overall normalization of the counts to cross section was made via the saturated resonance technique [9] using the 4.9-eV resonance in the ^{197}Au cross section. As described in Ref. [10], the capture apparatus has been improved in several significant ways as compared to the setup [11] used in most of the previous ORELA measurements. These changes have substantially reduced sample-dependent backgrounds and have improved the accuracy with which absolute cross sections can be determined. The changes have also simplified the calculation and improved the reliability of the pulse-height weighting functions, which must be used in the conversion of the counts to cross sections. These improvements were especially important in the current case because the capture cross section is much smaller and the sample-dependent backgrounds are potentially much larger than in any other of our previous measurements.

A ^6Li -loaded glass scintillator, located 43 cm ahead of the sample in the neutron beam, was used to measure the energy dependence of the neutron flux. Separate sample-out background measurements were made, and measurements with a carbon sample were used to subtract the smoothly varying background caused by the sample-scattered neutrons.

Two separate transmission measurements were made on ORELA flight path 1. In one measurement, a ^6Li -loaded glass scintillator was used at a source-to-detector distance of 80.117 m, and the sample was 0.0543 at/b thick. The ORELA was operated at a pulse rate of 400 Hz, a pulse width of 16 ns, and a power of 12 kW. In the other measurement, a plastic scintillation detector was used at a source-to-sample distance of 201.575 m, and the sample was 0.110 at/b thick. The ORELA was operated at a pulse rate of 577 Hz, a pulse width of 4 ns, and a power of 4 kW. In both measurements, a ^{10}B filter was used to remove overlap neutrons from preceding beam bursts. In the 80-m measurement, a Pb filter was used to reduce the effects caused by the γ flash at the beginning of each pulse from the ORELA, while a U filter was used for this purpose during the 200-m measurement. These filters were placed in the beam at a distance of 5 m from the neutron source. The strontium sample was exchanged periodically with an empty container, which had the same dimensions as the sample holder, and with polyethylene and bismuth absorbers, which were used for determination of backgrounds.

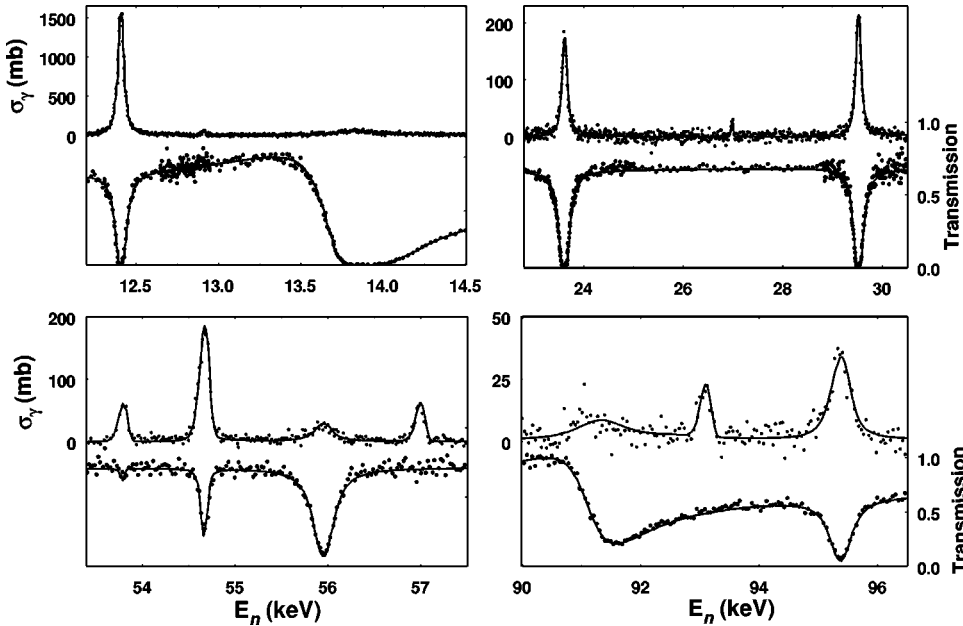


FIG. 2. Representative data (points) and SAMMY fits (solid curves) from our capture (top) and transmission (bottom) measurements on ^{88}Sr . The effective capture cross sections have not been corrected for finite-thickness effects. The corrections are included by the code SAMMY; hence, the fits represent the theoretical cross sections, calculated from the resonance parameters, after adjustment for these sample-dependent effects. The scales for the capture data are on the left of each plot, whereas the transmission scales are on the right.

III. RESONANCE ANALYSIS

The multilevel, multichannel, \mathcal{R} -matrix code SAMMY [12] was used to fit both our transmission and capture data and extract resonance parameters. Orbital angular momenta up to and including f waves were included in the analysis. Channel radii of 7.1 fm were used for all partial waves.

Resonances in both the neutron-capture and transmission data could be fitted from 100 eV to 350 keV. Below this range, the neutron flux on the sample was too low because of the ^{10}B overlap filter. Above 350 keV, both the statistical precision and the energy resolution in the neutron capture data were too poor to be able to include them in the resonance analysis. The 80-m transmission data were fitted for energies below 160 keV. The 200-m transmission data were fitted at higher energies because both the resolution and the statistical precision of these data were better than those of the 80-m data in this region. Using SAMMY, we determined the parameters for 101 resonances in the energy range below 350 keV. Representative data and fits are shown in Fig. 2. The resonance parameters are given in Table I.

Firm l and J^π values could be determined for resonances which were sufficiently strong in the transmission data. Using the fitted parameters of these firm assignments, we determined average radiation widths of 190 ± 120 , 220 ± 230 , and 280 ± 210 meV for $s_{1/2}$ (13 resonances), $p_{1/2}$ (eight resonances), and $p_{3/2}$ (18 resonances) resonances, respectively. The uncertainties quoted are the standard deviations of the distributions of the radiation widths. For weaker resonances or for those resonances which were visible in only the capture or the transmission data, there is some arbitrariness in determining the resonance parameters. In an attempt to minimize the arbitrariness of these parameters, the prescription outlined in Ref. [10] was followed. For example, for resonances that could be seen in the capture but not the transmission data, the radiation widths were fixed to the average values given previously while the capture data were fitted by letting the neutron width vary. In all these cases, the neutron

widths obtained by fitting the capture data were consistent with the transmission data. Originally [13], we had used the resonance parameters in Ref. [14] in the energy range above 350 keV as background levels—except that we allowed the neutron widths of some of the broader resonances in this region to vary to obtain better fits to the data below 350 keV. We have since used our transmission data to obtain better resonance parameters in the 350–950-keV region, resulting in parameters for 342 resonances in this region. The radiation widths for s - and p -wave resonances were fixed at the average values previously given. In addition, the radiation widths for resonances of all the other partial waves were set equal to 280 meV. We decided to terminate the fitting at 950 keV because of the sheer number of overlapping resonances and the strong interference effects. Above 900 keV, we did not attempt to fit the narrower resonances. Representative data and fits are shown in Fig. 3, where it can be seen that our new parameters represent a substantial improvement over previous results. The parameters for resonances in this range are given in Table II.

Given the excellent energy resolution at ORELA and the large resonance spacing in $n + ^{88}\text{Sr}$, we might expect to miss or spuriously assign few resonances. If the resonance parameter set can be shown to be relatively complete, then it would be useful for testing various models. However, we find that except for s waves, the firmness of the (lJ) assignments are less than satisfactory. Nevertheless, we report average resonance parameters for both s and p waves because our data and analysis are more extensive than any previous work.

The distinctive interference shape of the s -wave resonances allowed for much more reliable (lJ) assignments than for the higher l partial waves. A plot of the number of observed resonances versus energy for the s waves is linear up to about 700 keV, indicating few missing or spuriously assigned resonances. To estimate the number of missing or spuriously assigned resonances, we used two tests. First, we fitted the subset of the s -wave resonances, with reduced neu-

TABLE I. ^{88}Sr resonance parameters in the region below 350 keV, where we fitted both our neutron capture and transmission data. Note that, in the second column, two times the total angular momentum of each resonance is listed.

| E_n (keV) | $2J^\pi$ | $g\Gamma_n$ (eV) | Γ_γ (meV) | $g\Gamma_n\Gamma_\gamma/\Gamma$ (meV) |
|----------------|------------------|---------------------|--------------------------|--|
| 12.41 | (1) ⁻ | 20.86±0.16 | 446.2±6.1 | 436.9±5.8 |
| 12.91 | (1) ⁻ | 0.0048±0.0009 | 220 | 4.67±0.83 |
| 13.84 | 1 ⁺ | 194.15±0.54 | 80.5±7.4 | 80.5±7.4 |
| 18.21 | (3) ⁻ | 0.0017±0.0008 | 280 | 1.68±0.80 |
| 20.81 | (1) ⁻ | 0.0897±0.0054 | 220 | 63.7±2.7 |
| 23.61 | 3 ⁻ | 132.14±0.87 | 131.5±4.8 | 262.5±9.6 |
| 26.98 | (1) ⁻ | 0.0105±0.0025 | 220 | 10.1±2.2 |
| 29.52 | 3 ⁻ | 137.0±1.2 | 198.9±6.5 | 397±13 |
| 36.78 | (1) ⁻ | 0.0679±0.0082 | 220 | 51.9±4.7 |
| 39.07 | (1) ⁻ | 3.89±0.47 | 84.2±6.3 | 82.4±6.1 |
| 40.15 | (1) ⁻ | 0.099±0.012 | 220 | 68.2±5.6 |
| 46.47 | (1) ⁻ | 0.118±0.018 | 220 | 76.8±7.4 |
| 47.95 | (3) ⁻ | 0.151±0.014 | 280 | 119.2±9.0 |
| 48.57 | 1 ⁺ | 7.97±0.68 | 66.3±7.7 | 65.7±7.6 |
| 53.79 | (1) ⁻ | 2.24±0.55 | 110±11 | 105±10 |
| 54.66 | (3) ⁻ | 38.5±1.4 | 221.1±7.8 | 437±15 |
| 55.95 | 1 ⁻ | 146.3±2.0 | 79±12 | 79±12 |
| 56.99 | (3) ⁻ | 0.126±0.012 | 280 | 103.2±7.7 |
| 58.90 | (1) ⁺ | 2.03±0.64 | 23.4±5.1 | 23.1±5.0 |
| 65.48 | (1) ⁻ | 0.083±0.014 | 220 | 60.4±7.2 |
| 73.77 | (3) ⁻ | 0.090±0.013 | 280 | 77.9±9.6 |
| 75.50 | (3) ⁻ | 0.360±0.098 | 300±130 | 224±13 |
| 76.89 | (3) ⁻ | 0.118±0.018 | 280 | 98±12 |
| 88.56 | 3 ⁻ | 421.7±6.2 | 99±11 | 197±22 |
| 91.34 | 1 ⁺ | 953±13 | 273±33 | 273±33 |
| 93.08 | (3) ⁻ | 0.139±0.021 | 280 | 111±14 |
| 95.37 | 3 ⁻ | 447.9±7.5 | 227±20 | 453±41 |
| 101.95 | (3) ⁻ | 0.122±0.024 | 280 | 100±16 |
| 105.46 | 1 ⁺ | 256.2±7.1 | 305±26 | 305±26 |
| 107.45 | (3) ⁻ | 0.143±0.024 | 280 | 114±16 |
| 110.15 | 1 ⁻ | 284.9±8.4 | 146±28 | 146±28 |
| 115.92 | (3) ⁻ | 0.150±0.029 | 280 | 118±19 |
| 117.15 | (1) ⁻ | 0.091±0.034 | 220 | 64±17 |
| 120.10 | (1) ⁻ | 0.058±0.028 | 220 | 46±16 |
| 122.29 | 3 ⁻ | 3111±23 | 625±39 | 1249±77 |
| 125.95 | (3) ⁻ | 0.129±0.029 | 280 | 105±19 |
| 126.40 | (3) ⁻ | 0.189±0.038 | 280 | 141±22 |
| 127.90 | (3) ⁻ | 0.301±0.058 | 280 | 196±26 |
| 132.85 | (3) ⁻ | 0.152±0.036 | 280 | 119±23 |
| 137.35 | (3) ⁻ | 0.121±0.030 | 280 | 99±21 |
| 141.68 | 1 ⁺ | 501±13 | 79±29 | 79±29 |
| 147.30 | (3) ⁻ | 0.226±0.042 | 280 | 161±23 |
| 150.20 | (3) ⁻ | 43.4±7.2 | 84±20 | 166±40 |
| 150.87 | 1 ⁻ | 1205±24 | 703±87 | 702±87 |
| 153.89 | 3 ⁻ | 558±12 | 85±21 | 171±42 |
| 156.00 | (3) ⁻ | 0.191±0.042 | 280 | 142±25 |
| 160.85 | (3) ⁻ | 0.227±0.069 | 280 | 161±34 |
| 169.85 | (3) ⁻ | 0.105±0.039 | 280 | 88±27 |
| 170.79 | 3 ⁻ | 662.9±5.0 | 91±24 | 182±48 |

TABLE I. (*Continued*).

| E_n (keV) | $2J^\pi$ | $g\Gamma_n$ (eV) | Γ_γ (meV) | $g\Gamma_n\Gamma_\gamma/\Gamma$ (meV) |
|----------------|-------------------|---------------------|--------------------------|--|
| 173.38 | (3 ⁻) | 2.06±0.29 | 339±41 | 509±50 |
| 177.85 | (3 ⁻) | 6.3±1.1 | 196±21 | 370±38 |
| 181.06 | 1 ⁺ | 176.3±2.6 | 100±36 | 100±36 |
| 186.87 | (1 ⁻) | 4.88±0.45 | 114±36 | 111±34 |
| 187.62 | (3 ⁻) | 5.36±0.51 | 202±29 | 376±50 |
| 192.85 | (3 ⁻) | 0.198±0.056 | 280 | 146±34 |
| 194.81 | 1 ⁺ | 47.4±2.9 | 166±50 | 166±49 |
| 195.23 | 3 ⁻ | 2214.6±8.7 | 173±43 | 347±85 |
| 200.67 | 1 ⁻ | 425.3±4.5 | 78±29 | 78±29 |
| 202.53 | (1) ⁻ | 16.1±1.5 | 81±23 | 80±23 |
| 204.21 | 3 ⁻ | 151.3±2.6 | 240±22 | 479±44 |
| 212.13 | (3 ⁻) | 0.367±0.075 | 280 | 222±31 |
| 214.29 | 3 ⁻ | 1000.0±5.5 | 191±24 | 382±48 |
| 224.76 | (3 ⁻) | 3.82±0.47 | 153±24 | 283±41 |
| 225.19 | (1 ⁻) | 8.53±0.78 | 58±26 | 57±26 |
| 227.69 | 1 ⁻ | 364.5±6.9 | 415±60 | 415±59 |
| 228.29 | 3 ⁻ | 1885.4±9.5 | 94±32 | 188±65 |
| 230.20 | 1 ⁺ | 1452±10 | 419±71 | 419±71 |
| 232.93 | (1 ⁻) | 0.92±0.51 | 152±33 | 131±26 |
| 235.76 | (1 ⁻) | 15.7±1.1 | 56±23 | 56±23 |
| 241.08 | (1 ⁻) | 10.23±0.92 | 117±32 | 115±31 |
| 245.11 | (1 ⁻) | 9.3±1.5 | 281±46 | 273±43 |
| 246.06 | (1 ⁻) | 10.9±1.9 | 126±38 | 124±37 |
| 247.03 | 3 ⁻ | 3620±11 | 571±47 | 1141±93 |
| 252.02 | (3 ⁻) | 0.197±0.050 | 280 | 145±29 |
| 256.24 | (1 ⁻) | 29.0±1.5 | 187±36 | 186±35 |
| 258.67 | 1 ⁺ | 476.3±4.4 | 339±88 | 339±88 |
| 258.99 | 3 ⁻ | 48.1±2.1 | 319±44 | 629±85 |
| 265.06 | 1 ⁺ | 153.5±2.7 | 98±31 | 98±31 |
| 266.53 | 3 ⁺ | 50.5±2.0 | 121±37 | 241±73 |
| 267.96 | (1 ⁻) | 7.0±1.8 | 67±33 | 67±33 |
| 270.60 | (3 ⁻) | 0.187±0.054 | 280 | 140±31 |
| 277.64 | (1 ⁻) | 7.1±1.5 | 615±72 | 566±61 |
| 278.79 | 3 ⁻ | 71.5±2.6 | 128±24 | 255±49 |
| 281.63 | (3 ⁻) | 0.76±0.33 | 280±83 | 322±79 |
| 287.47 | (3 ⁻) | 14.6±6.8 | 680±130 | 1240±220 |
| 289.49 | 3 ⁻ | 24932±31 | 718±96 | 1440±190 |
| 297.82 | (1 ⁻) | 11.8±1.8 | 70±26 | 70±26 |
| 298.04 | (1 ⁻) | 12.5±1.7 | 54±21 | 54±21 |
| 302.08 | 1 ⁺ | 232.8±3.6 | 297±70 | 296±70 |
| 302.96 | 3 ⁻ | 2517.0±9.4 | 479±61 | 960±120 |
| 308.13 | (1) ⁻ | 96.5±2.5 | 68±30 | 68±30 |
| 310.96 | (1 ⁻) | 5.8±1.2 | 286±52 | 273±48 |
| 318.81 | 1 ⁺ | 21.2±1.6 | 178±44 | 177±43 |
| 322.67 | 1 ⁻ | 183.8±5.0 | 182±44 | 182±44 |
| 325.30 | 3 ⁻ | 22082±29 | 572±97 | 1140±190 |
| 329.40 | 3 ⁺ | 211.4±5.7 | 27±6 | 54±31 |
| 330.04 | (1 ⁻) | 23.4±3.0 | 29±18 | 29±18 |
| 334.33 | 1 ⁻ | 90.2±3.1 | 92±31 | 92±31 |
| 340.12 | (1 ⁺) | 3.2±1.2 | 100±47 | 97±44 |
| 344.33 | 3 ⁻ | 4053±12 | 90±33 | 181±66 |
| 347.29 | 1 ⁺ | 202.0±3.7 | 64±23 | 64±23 |

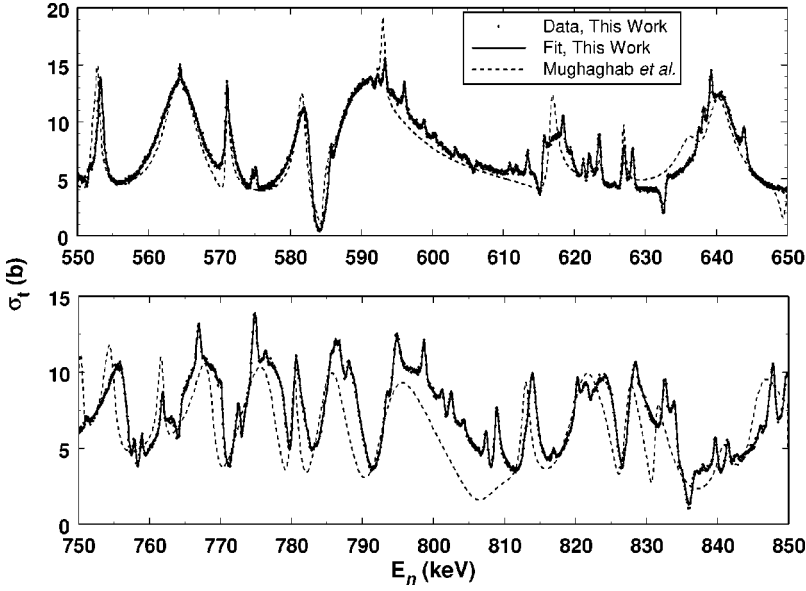


FIG. 3. Representative data (points) and SAMMY fits (solid curves) to our total cross section data in the region from 350 to 950 keV. Shown for comparison is the total cross section calculated using the resonance parameters of Ref. [14] (dashed curves).

neutron widths larger than one-fourth the average reduced neutron width, to a Porter-Thomas (PT) distribution [15–17]. The average reduced width for the optimal PT distribution provides a measure of the population's mean reduced width, and, therefore, provides an estimate for the number of missed resonances. The results of this test for $s_{1/2}$ resonances are shown in Fig. 4. Extrapolation of the fitted PT curve to zero reduced width yields the estimate of no missing s -wave resonances over the range of our measurement. A second test for missing or spuriously assigned resonances for which incorrect (IJ) assignments have been made is provided by the Δ_3 test of Dyson and Mehta [18]. Up to a neutron energy of 450 keV, the observed value of the Δ_3 statistic is consistent with no missed or spuriously identified $s_{1/2}$ resonances. Inclusion of a 58.90-keV resonance in the $s_{1/2}$ resonance set produces values of Δ_3 within one standard deviation of the expected value. Hence, this narrow resonance could be an s wave. Above 450 keV, the Δ_3 test implies that a few s -wave resonances are missed or spuriously assigned as $\frac{1}{2}^+$. Because the s -wave assignments appear to be rather firm, the correlation coefficient, $\rho(\gamma_\lambda^2, \Gamma_{\gamma\lambda})$, between the neutron widths and γ -partial widths can be calculated with some confidence. Significant correlation coefficients have been interpreted [5] as evidence for the applicability of the valence model of neutron capture [19]. From our fitted parameters for s -wave resonances, we calculate that $\rho = (0.23 \pm 0.06)$. Drawing reduced neutron widths from a PT distribution with $\langle \gamma_\lambda^2 \rangle$ equal to that for the observed s -wave resonances and radiation widths from a χ^2 distribution with 18 degrees of freedom, we find a likelihood of exceeding this value of ρ of about 6%.

The situation for the p -wave resonance (IJ) assignments is much less satisfactory. The difficulty is that below about 350 keV the shapes of the $p_{1/2}$ and $p_{3/2}$ resonances are very similar. Despite the excellent ORELA energy resolution, distinguishing between the $p_{1/2}$ and $p_{3/2}$ resonances is possible only for the widest p waves. If the assignments shown in Table I are assumed correct, the Δ_3 test indicates no missed

or spuriously assigned $p_{1/2}$ resonances only up to 75 keV and no missed or spuriously assigned $p_{3/2}$ resonances up to 150 keV. The PT tests are consistent with 8 missing $p_{1/2}$ and 10 missing $p_{3/2}$ resonances, although the observed distributions, as shown in Fig. 4, are not in good agreement with the expected PT distributions. If we assume that the 35 $p_{1/2}$ and 49 $p_{3/2}$ resonances have been correctly assigned and that few small resonances are missed in our work, we can calculate the correlation coefficients. For the 35 $p_{1/2}$ resonances, we find $\rho = (0.55 \pm 0.09)$. Drawing γ_λ^2 from a PT distribution with a mean equal to that observed and Γ_γ from a χ_ν^2 with 3 degrees of freedom, we find that the likelihood of exceeding this value of ρ is less than 1%. For the 49 $p_{3/2}$ resonances identified in our work up to 350 keV, we find $\rho = (0.59 \pm 0.09)$. The probability of exceeding $\rho = 0.59$ is less than 1%.

Because few s -wave resonances up to 450 keV appear to have been missed or spuriously assigned in this work, the s -wave level spacing is calculated using resonances below that energy. The resulting s -wave spacing is $D_{0(1/2)} = (23.7 \pm 2.9)$ keV. Even though the (IJ) assignments for the p -wave resonances below 350 keV can be made unambiguously in only a few cases, we are confident that, in most cases, at higher energies the l assignments are reasonably firm. Hence, we included all the p -wave resonances to calculate an average resonance spacing (5.4 ± 0.2) keV.

The observed neutron strength functions s_{IJ} are defined as

$$s_{IJ} = \frac{\langle \gamma_{\lambda IJ}^2 \rangle}{D_{IJ}} = \frac{N^{obs} - 1}{N^{obs}} \frac{\sum_\lambda \gamma_{\lambda IJ}^2}{\Delta E_{IJ}}, \quad (1)$$

where the ΔE_{IJ} are the energy intervals between the lowest- and highest-energy resonances of type (IJ). The angle-bracket notation indicates the averaging process. The s_{IJ} are approximately the slopes of the cumulative reduced width versus energy distributions, as shown in Fig. 5 for the $s_{1/2}$, $p_{1/2}$, and $p_{3/2}$ resonances. The s_{IJ} values were determined

TABLE II. ^{88}Sr resonance parameters for the region above 350 keV.

| E_n (keV) | $2J^\pi$ | $g\Gamma_n$ (eV) | E_n (keV) | $2J^\pi$ | $g\Gamma_n$ (eV) | E_n (keV) | $2J^\pi$ | $g\Gamma_n$ (eV) |
|----------------|----------|---------------------|----------------|------------|---------------------|----------------|----------|---------------------|
| 350.86 | 1^- | 47.7 ± 2.5 | 491.42 | (3^+) | 64.6 ± 3.5 | 613.46 | (5^-) | 148.9 ± 5.1 |
| 353.64 | 1^- | 17.1 ± 2.2 | 492.81 | 3^- | 3258 ± 14 | 615.30 | 1^+ | 470 ± 10 |
| 355.03 | 1^- | 472.7 ± 5.4 | 494.78 | (3^+) | 54.1 ± 3.2 | 615.79 | (3^+) | 102.5 ± 5.7 |
| 358.98 | 1^- | 44.7 ± 2.2 | 497.31 | (3^+) | 33.4 ± 2.9 | 616.96 | 1^- | 5071 ± 40 |
| 364.88 | 3^- | 990.4 ± 6.0 | 502.47 | (3^-) | 2762 ± 14 | 618.45 | (7^-) | 168.4 ± 6.6 |
| 368.18 | 1^- | 158.1 ± 4.6 | 505.92 | (5^+) | 13.3 ± 2.9 | 619.55 | (5^-) | 58.4 ± 6.6 |
| 368.30 | 3^- | 140.5 ± 3.3 | 506.14 | 1^- | 3699 ± 28 | 620.89 | (3^+) | 28.5 ± 4.2 |
| 370.21 | 3^- | 33.5 ± 2.2 | 506.52 | (3^+) | 11.5 ± 2.3 | 621.20 | (1^-) | 156.9 ± 6.4 |
| 373.57 | 3^- | 28.1 ± 2.1 | 506.93 | (5^-) | 15.8 ± 3.3 | 621.99 | (1^-) | 22.1 ± 7.6 |
| 377.70 | 3^- | 154.6 ± 3.0 | 507.36 | (5^+) | 15.5 ± 4.1 | 623.19 | (1^-) | 60.1 ± 7.1 |
| 379.46 | 3^- | 68.1 ± 2.7 | 509.33 | (5^-) | 25.3 ± 3.2 | 623.58 | (3^+) | 346 ± 10 |
| 382.29 | 3^- | 706.3 ± 5.5 | 513.79 | (3^+) | 136.4 ± 4.7 | 625.72 | (5^-) | 22.2 ± 3.7 |
| 385.85 | 1^- | 938 ± 11 | 516.50 | 1^+ | 584.1 ± 9.7 | 626.95 | (5^-) | 170 ± 16 |
| 386.08 | 3^- | 4395 ± 14 | 521.03 | 1^- | 14568 ± 849 | 627.09 | (5^-) | 187.5 ± 9.6 |
| 392.24 | 1^+ | 24.4 ± 1.8 | 520.92 | 3^- | 43008 ± 65 | 628.24 | (3^+) | 317 ± 6.0 |
| 400.58 | 3^- | 332.9 ± 4.4 | 522.21 | (5^-) | 101.6 ± 6.5 | 632.67 | 1^+ | 339.4 ± 7.1 |
| 403.96 | 1^- | 6158 ± 23 | 524.90 | 3^- | 1146 ± 30 | 637.58 | (5^-) | 116.4 ± 5.8 |
| 408.46 | (5^-) | 31.8 ± 2.6 | 528.84 | (7^-) | 239.8 ± 6.0 | 638.20 | (5^-) | 194.3 ± 6.3 |
| 409.11 | (3^+) | 39.3 ± 2.8 | 530.58 | (5^-) | 115.1 ± 4.9 | 639.07 | (7^-) | 82.5 ± 8.9 |
| 409.28 | (5^-) | 116.5 ± 3.5 | 531.75 | (3^+) | 7.7 ± 2.6 | 639.30 | (7^-) | 280.3 ± 9.7 |
| 409.82 | (5^+) | 10.9 ± 2.2 | 532.86 | (5^-) | 236.4 ± 5.3 | 639.53 | 3^- | 12432 ± 40 |
| 410.11 | 3^- | 357.9 ± 4.7 | 533.66 | (7^-) | 11.7 ± 4.8 | 643.88 | 1^- | 395 ± 11 |
| 418.86 | 1^+ | 478.5 ± 6.0 | 535.26 | 3^- | 2203 ± 14 | 652.13 | (5^-) | 87.0 ± 5.6 |
| 422.45 | (3^+) | 1913 ± 13 | 536.66 | 1^- | 10997 ± 65 | 6522.44 | (5^-) | 109.4 ± 5.6 |
| 422.64 | 1^+ | 22.4 ± 2.9 | 542.43 | 3^- | 3048 ± 20 | 655.83 | 1^+ | 42.3 ± 3.8 |
| 422.90 | 1^- | 109.2 ± 6.1 | 542.60 | (5^+) | 49.3 ± 5.8 | 656.60 | (5^-) | 31.2 ± 4.3 |
| 423.30 | 1^- | 95.3 ± 4.4 | 544.62 | (5^-) | 27.0 ± 5.3 | 659.84 | 1^- | 303.6 ± 9.5 |
| 426.87 | (3^+) | 63.7 ± 2.9 | 545.53 | 3^- | 2182 ± 15 | 660.68 | 1^- | 140 ± 6.8 |
| 430.58 | (5^-) | 30.2 ± 3.9 | 551.43 | 1^+ | 51.5 ± 3.0 | 662.09 | 3^- | 2952 ± 21 |
| 430.69 | 3^- | 1135.9 ± 8.1 | 553.15 | 3^- | 1918 ± 18 | 664.62 | (5^-) | 115.9 ± 5.8 |
| 432.86 | (3^+) | 114.6 ± 3.4 | 563.44 | 3^- | 14878 ± 32 | 666.29 | 3^- | 13906 ± 53 |
| 436.09 | 1^- | 374.5 ± 6.7 | 564.47 | (5^+) | 84.7 ± 5.3 | 670.69 | 1^+ | 336 ± 12 |
| 437.92 | 1^- | 13.7 ± 2.7 | 571.05 | (5^+) | 382.6 ± 3.2 | 671.15 | (7^-) | 131.3 ± 6.6 |
| 441.32 | 1^+ | 718.8 ± 9.5 | 570.61 | 3^+ | 16.3 ± 6.0 | 672.62 | (7^-) | 446.9 ± 5.2 |
| 441.65 | 3^- | 16403 ± 33 | 571.18 | 1^- | 1759 ± 16 | 673.09 | (5^-) | 44.2 ± 5.0 |
| 446.25 | 1^- | 118.5 ± 5.0 | 574.72 | 7^- | 76.7 ± 3.7 | 673.89 | (7^-) | 50.3 ± 5.1 |
| 447.04 | 1^- | 66.8 ± 4.0 | 575.19 | (5^-) | 105.8 ± 5.2 | 674.40 | (5^-) | 182.8 ± 5.6 |
| 455.76 | 1^+ | 6.8 ± 1.7 | 581.55 | 3^- | 7198 ± 26 | 676.17 | (5^-) | 141.6 ± 5.3 |
| 458.35 | (3^+) | 229.5 ± 3.9 | 584.81 | 1^+ | 3132 ± 29 | 676.76 | (7^-) | 40.3 ± 4.5 |
| 460.09 | 1^+ | 20.1 ± 2.1 | 585.72 | (3^+) | 177.7 ± 5.5 | 677.52 | (5^-) | 51.0 ± 4.9 |
| 466.11 | 1^- | 38.4 ± 3.3 | 589.46 | 3^- | 23370 ± 46 | 678.11 | (5^-) | 49.4 ± 5.0 |
| 469.38 | (3^+) | 411.1 ± 4.6 | 591.94 | 3^- | 260 ± 21 | 678.64 | (7^-) | 273.3 ± 7.0 |
| 475.49 | 3^- | 899.4 ± 7.4 | 592.32 | (5^-) | 38.8 ± 5.0 | 680.22 | 3^- | 8295 ± 45 |
| 477.07 | (5^+) | 65.7 ± 4.0 | 593.40 | (3^+) | 193.3 ± 6.2 | 681.19 | (7^-) | 135.3 ± 8.5 |
| 477.62 | 1^+ | 374.1 ± 7.5 | 596.11 | (3^+) | 182.9 ± 5.9 | 681.52 | (5^-) | 156.5 ± 8.4 |
| 480.86 | (3^+) | 54.1 ± 3.1 | 598.88 | (5^-) | 66.7 ± 5.5 | 682.23 | (5^-) | 60.2 ± 6.5 |
| 485.30 | 1^- | 196.3 ± 6.2 | 600.41 | (7^-) | 51.1 ± 5.2 | 682.85 | (5^-) | 40.3 ± 5.9 |
| 486.74 | (5^-) | 253.7 ± 7.6 | 603.12 | (3^-) | 43.2 ± 4.1 | 684.72 | (7^-) | 282.9 ± 7.2 |
| 486.96 | 1^- | 133.1 ± 9.0 | 604.65 | (7^{-1}) | 40.9 ± 6.3 | 686.40 | 1^+ | 21.6 ± 4.0 |
| 487.18 | (5^-) | 35.2 ± 3.9 | 605.90 | 1^+ | 53.9 ± 3.6 | 687.25 | 1^+ | 29.5 ± 4.1 |
| 487.54 | (3^+) | 15.0 ± 3.4 | 611.00 | (3^+) | 48.3 ± 4.2 | 687.79 | 1^+ | 29.4 ± 4.1 |
| 487.58 | 3^- | 3688 ± 15 | 611.87 | (3^+) | 48.9 ± 4.2 | 688.32 | (5^-) | 15.1 ± 3.8 |

TABLE II. (*Continued*).

| E_n (keV) | $2J^\pi$ | $g\Gamma_n$ (eV) | E_n (keV) | $2J^\pi$ | $g\Gamma_n$ (eV) | E_n (keV) | $2J^\pi$ | $g\Gamma_n$ (eV) |
|----------------|-------------------|---------------------|----------------|-------------------|---------------------|----------------|-------------------|---------------------|
| 689.93 | (7 ⁻) | 82.8±5.5 | 767.04 | (5 ⁻) | 412±11 | 828.50 | (5 ⁻) | 119.3±8.5 |
| 693.42 | 1 ⁻ | 1039±66 | 767.71 | (5 ⁻) | 75.6±8.1 | 832.60 | (5 ⁻) | 576±13 |
| 693.46 | 1 ⁺ | 57.7±7.7 | 770.42 | (1 ⁺) | 112±13 | 833.17 | 1 ⁻ | 1331±55 |
| 694.33 | (7 ⁻) | 201±13 | 770.04 | (7 ⁻) | 120±33 | 834.00 | 5 ⁻ | 395±19 |
| 694.90 | (5 ⁻) | 324±21 | 770.28 | 7 ⁻ | 308±53 | 836.11 | (1 ⁺) | 1163±23 |
| 694.57 | (7 ⁻) | 316±27 | 772.62 | 3 ⁻ | 1655±37 | 837.36 | 1 ⁺ | 72.4±7.3 |
| 695.03 | (5 ⁺) | 140±16 | 774.70 | (3 ⁻) | q19405±13 | 838.50 | (1 ⁺) | 36.4±5.8 |
| 695.83 | 1 ⁺ | 28.1±4.3 | 774.55 | 5 ⁻ | 210±110 | 839.69 | (5 ⁻) | 299.8±8.3 |
| 696.88 | 1 ⁻ | 12074±90 | 774.88 | 5 ⁻ | 663±14 | 840.54 | (1 ⁺) | 75.2±6.2 |
| 696.95 | (7 ⁻) | 40.2±5.5 | 775.81 | (7 ⁻) | 440±7.0 | 841.47 | 7 ⁻ | 213.4±8.1 |
| 697.43 | (5 ⁻) | 68.9±6.4 | 776.38 | (7 ⁻) | 116.9±8.3 | 842.67 | (7 ⁻) | 25.2±5.9 |
| 697.81 | (7 ⁻) | 98.0±7.6 | 780.50 | 3 ⁻ | 2285±15 | 846.03 | (7 ⁻) | 101.2±8.0 |
| 698.23 | (7 ⁻) | 139.4±8.4 | 780.24 | 1 ⁻ | 534±26 | 847.53 | (3 ⁺) | 391±12 |
| 698.65 | (5 ⁻) | 90.0±7.6 | 781.90 | (5 ⁻) | 101±11 | 847.90 | 7 ⁻ | 770±11 |
| 699.04 | 3 ⁻ | 3054±34 | 782.38 | (7 ⁻) | 174.6±9.3 | 849.61 | (5 ⁺) | 215±11 |
| 699.38 | 1 ⁺ | 52.2±6.6 | 782.82 | (7 ⁻) | 147.0±8.2 | 850.28 | 3 ⁺ | 1503±22 |
| 700.12 | (5 ⁻) | 56.4±9.3 | 783.30 | (5 ⁻) | 125.7±7.9 | 850.98 | (1 ⁺) | 1620±33 |
| 704.17 | 1 ⁺ | 34.0±4.6 | 785.31 | 3 ⁻ | 12002±67 | 851.97 | 3 ⁻ | 38570±140 |
| 704.78 | (5 ⁻) | 44.9±5.9 | 785.55 | (5 ⁻) | 191.1±8.8 | 853.26 | (7 ⁻) | 71.0±8.9 |
| 705.48 | (5 ⁻) | 44.2±6.4 | 786.19 | (7 ⁻) | 262±11 | 861.36 | 5 ⁻ | 113.8±9.0 |
| 706.09 | (5 ⁻) | 335.2±8.2 | 786.74 | (7 ⁻) | 250±10 | 862.31 | (1 ⁺) | 60.9±7.2 |
| 708.65 | 3 ⁺ | 7394±44 | 788.40 | (3 ⁻) | 532±11 | 863.85 | (7 ⁻) | 64.0±8.7 |
| 709.71 | (7 ⁻) | 70.9±6.9 | 788.17 | 7 ⁻ | 460±23 | 866.75 | 1 ⁺ | 526±17 |
| 710.41 | (5 ⁻) | 92.5±7.1 | 793.44 | (5 ⁻) | 190.6±8.0 | 868.47 | (1 ⁺) | 53.2±7.1 |
| 714.57 | (5 ⁻) | 131.1±6.4 | 794.43 | (3 ⁻) | 14739.8±9.4 | 870.32 | (1 ⁺) | 38.3±6.4 |
| 715.89 | 1 ⁻ | 3064±33 | 794.34 | 5 ⁻ | 156±62 | 871.39 | 5 ⁻ | 78.9±8.2 |
| 716.98 | (5 ⁻) | 239.2±8.9 | 794.82 | (7 ⁻) | 428±12 | 872.12 | (7 ⁻) | 87.7±8.4 |
| 717.07 | 1 ⁺ | 490±16 | 795.31 | (7 ⁻) | 182±10 | 874.94 | 3 ⁺ | 3012±28 |
| 719.11 | (5 ⁻) | 144.4±8.5 | 798.66 | (5 ⁻) | 375.4±9.5 | 874.97 | (5 ⁻) | 120±0 |
| 719.53 | 3 ⁻ | 519±20 | 801.29 | (5 ⁻) | 129.1±8.7 | 877.72 | (7 ⁻) | 462±12 |
| 722.50 | (5 ⁺) | 154.5±6.9 | 801.88 | 1 ⁺ | 46.4±6.2 | 878.20 | (5 ⁻) | 860±16 |
| 723.10 | 3 ⁻ | 4633±27 | 802.51 | (5 ⁻) | 214.1±8.8 | 878.85 | 7 ⁻ | 255±10 |
| 724.38 | (5 ⁻) | 67.1±5.5 | 804.25 | (5 ⁻) | 102.1±7.8 | 880.07 | (5 ⁻) | 265.8±9.9 |
| 726.86 | (5 ⁻) | 40.2±5.5 | 807.41 | (7 ⁻) | 280.2±8.3 | 880.67 | (7 ⁻) | 521±11 |
| 731.13 | 3 ⁻ | 15094±43 | 808.71 | 3 ⁻ | 745±11 | 881.18 | (5 ⁻) | 539±12 |
| 731.63 | (5 ⁻) | 112.6±7.1 | 810.94 | 1 ⁺ | 29.1±5.6 | 881.78 | 7 ⁻ | 531±12 |
| 734.93 | (5 ⁻) | 53.9±5.6 | 811.72 | 1 ⁺ | 40.6±5.6 | 883.73 | (1 ⁺) | 19.6±7.4 |
| 739.52 | 3 ⁻ | 6431±28 | 812.87 | (7 ⁻) | 216.7±9.3 | 883.57 | (1 ⁺) | 17.8±7.4 |
| 739.67 | 1 ⁻ | 373±12 | 813.34 | (7 ⁻) | 272±11 | 884.37 | 7 ⁻ | 241.4±9.2 |
| 743.79 | 1 ⁺ | 718±14 | 813.76 | 3 ⁻ | 1306±20 | 885.22 | (1 ⁺) | 28.1±6.1 |
| 743.81 | 1 ⁻ | 20.4±5.0 | 814.26 | 1 ⁻ | 1482±32 | 887.65 | (5 ⁻) | 70.9±7.7 |
| 747.23 | (5 ⁻) | 61.6±5.5 | 815.55 | (5 ⁻) | 77.2±9.5 | 888.32 | (7 ⁻) | 82.8±8.4 |
| 751.12 | (5 ⁻) | 66.2±6.2 | 816.13 | (5 ⁻) | 48.9±7.4 | 889.16 | (5 ⁻) | 614±13 |
| 754.67 | 3 ⁻ | 15547±61 | 816.90 | (7 ⁻) | 133.3±7.8 | 889.71 | (5 ⁻) | 170±12 |
| 757.94 | (5 ⁻) | 230.0±7.0 | 820.23 | (5 ⁻) | 294.9±8.8 | 890.56 | 7 ⁻ | 891±14 |
| 758.90 | (5 ⁻) | 241.2±7.0 | 820.83 | 3 ⁻ | 10798±61 | 891.09 | 5 ⁻ | 484±12 |
| 761.83 | (5 ⁻) | 309.8±7.7 | 821.29 | 1 ⁺ | 15.5±6.2 | 891.68 | (7 ⁻) | 618±13 |
| 764.15 | 1 ⁺ | 408±11 | 821.68 | 1 ⁺ | 67.4±8.3 | 892.79 | 5 ⁻ | 207±14 |
| 765.62 | (5 ⁻) | 46.8±6.6 | 822.41 | (5 ⁻) | 501.7±9.7 | 893.15 | 5 ⁻ | 377±16 |
| 766.16 | (7 ⁻) | 64.7±7.8 | 822.97 | 3 ⁻ | 5434±45 | 893.83 | (3 ⁻) | 32920±150 |
| 766.26 | 3 ⁻ | 31360±170 | 823.82 | 1 ⁺ | 48.1±67 | 893.85 | (7 ⁻) | 133±11 |
| 766.63 | (7 ⁻) | 144.5±9.8 | 827.64 | 3 ⁻ | 4227±30 | 894.53 | 7 ⁻ | 97±13 |

TABLE II. (Continued).

| E_n (keV) | $2J^\pi$ | $g\Gamma_n$ (eV) | E_n (keV) | $2J^\pi$ | $g\Gamma_n$ (eV) | E_n (keV) | $2J^\pi$ | $g\Gamma_n$ (eV) |
|----------------|-------------------|---------------------|----------------|-------------------|---------------------|----------------|-------------------|---------------------|
| 895.50 | (7 ⁻) | 86±18 | 905.66 | 3 ⁻ | 885±17 | 933.82 | (7 ⁻) | 69±17 |
| 895.56 | 1 ⁺ | 326±29 | 911.42 | (7 ⁻) | 52.3±7.6 | 934.26 | (7 ⁻) | 1541±19 |
| 896.62 | (7 ⁻) | 119±10 | 931.76 | (7 ⁻) | 495±15 | 939.11 | (7 ⁻) | 1546±15 |
| 898.73 | (5 ⁻) | 91±21 | 913.88 | 1 ⁺ | 622±24 | 940.78 | 1 ⁺ | 79.8±7.6 |
| 899.09 | (7 ⁻) | 501±21 | 915.82 | (7 ⁻) | 301±10 | 942.29 | (7 ⁻) | 615±12 |
| 899.29 | 1 ⁺ | 517±60 | 917.05 | 1 ⁺ | 127.9±8.9 | 943.34 | 1 ⁺ | 199±11 |
| 899.44 | (5 ⁻) | 388±26 | 921.43 | (7 ⁻) | 113±96 | 944.20 | (7 ⁻) | 414±13 |
| 900.04 | (7 ⁻) | 83±14 | 920.49 | (3 ⁻) | 20346±11 | 945.42 | (7 ⁻) | 455±14 |
| 902.48 | 1 ⁺ | 237±13 | 928.44 | (7 ⁻) | 1226±13 | 947.56 | (7 ⁻) | 35±11 |
| 904.25 | (7 ⁻) | 324±13 | 930.38 | (3 ⁻) | 8637±59 | 948.23 | (3 ⁻) | 20270±210 |

from a linear fit to the observed cumulative reduced width distributions up to 450 keV for the s waves and up to 950 keV for the p waves. The resulting values are (0.010 ± 0.004) , (0.075 ± 0.014) , (0.22 ± 0.03) , respectively, for $s_{1/2}$, $p_{1/2}$, and $p_{3/2}$. Perhaps a more meaningful quantity to report for the p -wave resonances would be the strength function calculated by grouping all such resonances and using $g_J \gamma_\lambda^2$ rather than γ_λ^2 . The resulting p -wave strength function is (0.17 ± 0.02) . The observed strength functions should be corrected for the effects of missed resonances. However, in

the present work, these corrections are negligible for the s -wave resonances and not well known for the p waves.

The strength functions given above were calculated using \mathcal{R} -matrix reduced widths. The strength function which has been most often reported [14] in the earlier literature is the ratio

$$S_{IJ} = \frac{\langle \Gamma_{nJ}^I \rangle}{D_{IJ}}, \quad (2)$$

where the Γ_{nJ}^I are the conventionally reduced widths,

$$\Gamma_{nJ}^I = \left(\frac{1 \text{ eV}}{E_{\lambda IJ}} \right)^{1/2} \frac{\Gamma_{\lambda IJ}}{v_I}, \quad (3)$$

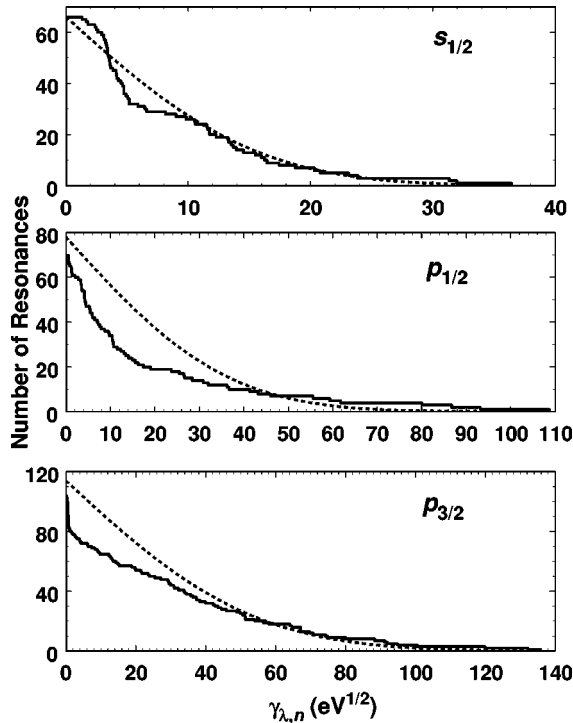


FIG. 4. PT distribution for s and p waves. Plotted are the number of resonances having a reduced width amplitude larger than a given size versus the size of the reduced width amplitude. In each subplot, the histogram shows the results from our resonance analysis, whereas the dashed curve shows the theoretical PT shape least-squares fitted to the data having reduced widths greater than 1/4 the average width.

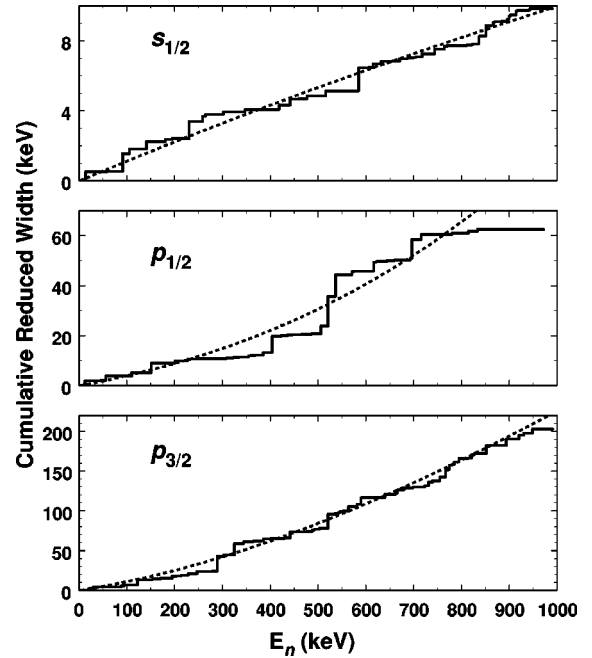


FIG. 5. Cumulative reduced width versus resonance energy for s - and p -wave resonances. The solid ‘‘staircase’’ curves are the cumulative reduced widths determined from our resonance analysis. The dashed curves are from the optical model fits to the data (see the text for details).

TABLE III. Parameters defining the external \mathcal{R} functions.

| l_J | a_{lJ} | b_{lJ} (eV $^{-1}$) | s_{lJ}^{ext} |
|-----------|-----------------------|------------------------|-----------------------|
| $s_{1/2}$ | -4.3×10^{-2} | 2.8×10^{-8} | 1.0×10^{-2} |
| $p_{1/2}$ | 0.45 | 3.2×10^{-7} | 7.5×10^{-2} |
| $p_{3/2}$ | 0.43 | -1.8×10^{-7} | 0.22 |
| $d_{3/2}$ | -0.70 | 2.3×10^{-6} | 4.1×10^{-2} |
| $d_{5/2}$ | -2.5 | 3.3×10^{-6} | 2.6×10^{-3} |
| $f_{5/2}$ | 1.0×10^{-3} | 4.6×10^{-7} | 0.24 |
| $f_{7/2}$ | 1.0×10^{-3} | 9.0×10^{-8} | 0.19 |

and the v_l are the neutron penetration factors [14] for partial waves with orbital angular momenta l . The strength functions S_{lJ} and s_{lJ} are related by

$$S_{lJ} = 4 \times 10^{-4} \frac{A}{A+1} a_c s_{lJ}, \quad (4)$$

where $a_c = 7.1$ fm (in this work). The relationship between S_{lJ} and s_{lJ} is discussed more fully in Ref. [20]. The value of the conventionally defined s -wave and p -wave strength functions from this work are $S_0 = (0.32 \pm 0.06) \times 10^{-4}$ and $S_1 = (5.1 \pm 0.6) \times 10^{-4}$.

In our analysis, the external \mathcal{R} -functions $R_{lJ}^{\text{ext}}(E)$, which represent the effects of resonances outside the fitted energy range ($E_{\text{low}} = 0$ to $E_{\text{up}} = 955$ keV), were parametrized as

$$R_{lJ}^{\text{ext}}(E) = \bar{R}_{lJ}(E) - s_{lJ}^{\text{ext}} \ln \frac{E_{\text{up}} - E}{E - E_{\text{low}}}. \quad (5)$$

This representation was used (i) because it has been found [21] to give a good average description of the effects of the external resonances, especially near the end points, where the effects of resonances just outside the fitted range are particularly important, and (ii) because it lends itself to interpretation in terms of the optical model. We parametrized $\bar{R}_{lJ}(E)$ by

$$\bar{R}_{lJ}(E) = a_{lJ} + b_{lJ}E, \quad (6)$$

where the coefficients a_{lJ} and b_{lJ} were free parameters determined in the fit to the data. The choice of s_{lJ}^{ext} followed an iterative procedure; it was finally chosen to give a good description of the observed average reduced neutron width per energy interval within the fitted energy range. In Table III are listed the values of a_{lJ} , b_{lJ} , and s_{lJ}^{ext} , which were derived from the \mathcal{R} -matrix analysis. The values of $R_{lJ}^{\text{ext}}(E)$, which were evaluated at a few energies, are shown in Fig. 6. Well depths for the spherical optical model potential (OMP) were least-squares adjusted to fit the observed R_{lJ}^{ext} and integrated strength (see Fig. 5) following the procedures of Ref. [21]. The summed strength was used because that statistic is relatively unaffected by a few missing small resonances. The resulting optical-model R_{lJ}^{ext} and integrated strength are compared to the values extracted from the \mathcal{R} -matrix analysis in Figs. 5 and 6. The fitted OMP real well depths are 50.2 ± 0.2 MeV and 53.5 ± 0.2 MeV for s and p waves, respec-

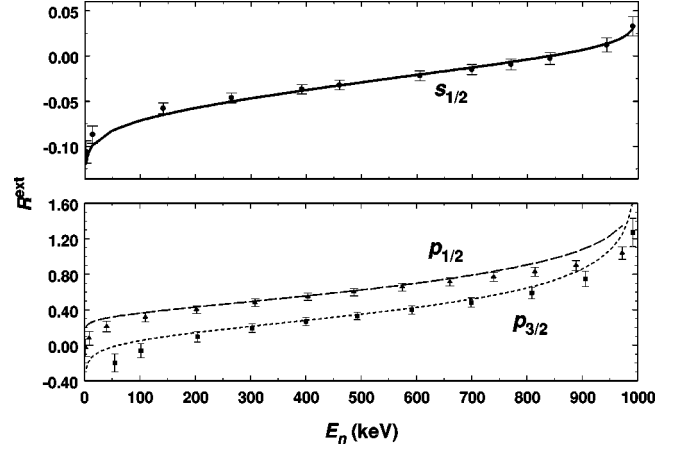


FIG. 6. Comparison of the R_{lJ}^{ext} functions from our resonance analysis (points with error bars) to those calculated by fitting an optical-model potential to these data (curves).

tively. The fitted surface imaginary well depths are 1.5 ± 0.1 MeV, 2.4 ± 0.3 MeV, and 4.2 ± 0.3 MeV for $s_{1/2}$, $p_{1/2}$, and $p_{3/2}$, respectively. A spin-orbit well depth $V_{so} = 8 \pm 1$ MeV was determined by requiring the same real well depth for both p -wave channels.

The s -wave potential scattering radius R' is determined from $\bar{R}_{0,1/2}(E)$, which was evaluated near $E = 0$,

$$R' = a_c [1 - \bar{R}_{0,1/2}(0)] = 6.8 \text{ fm}. \quad (7)$$

(Note that R' is independent of the value chosen for the channel radius a_c .)

IV. NEUTRON SENSITIVITY CORRECTION

Since the implementation of the new apparatus for (n, γ) measurements at ORELA [10], we have not made corrections to our resonance parameters for the background resulting from the prompt capture of scattered neutrons. In the old ORELA setup, this ‘‘neutron sensitivity’’ background could be substantial for resonances with large neutron widths. Since the change from C_6F_6 to C_6D_6 detectors, the replacement of the aluminum beam line and sample changer apparatus with a much less massive carbon fiber beam tube, and the elimination of the massive metallic cans which enclosed the detectors, this background has been reduced so much that it so far has been immeasurable. However, the relatively large level spacing and small cross section for $^{88}\text{Sr}(n, \gamma)$ allow us to make a good determination of the upper limit for this background. The data show that the prompt neutron sensitivity of the ORELA apparatus is much smaller than that of any other similar apparatus for which data have been published and that the corrections due to this effect are very small or negligible in all cases we have studied to date, thus justifying our lack of corrections to previous data. To calculate the size of this background, we compared our data to measurements on $^{208}\text{Pb}(n, \gamma)$ [22] and $^{88}\text{Sr}(n, \gamma)$ [7], which were made with a similar apparatus at Geel. In Ref. [22], time-of-flight peaks at 27.05 and 34.75 keV, due to the prompt capture of neutrons scattered from the ^{208}Pb sample

by the fluorine and aluminum housing of the C_6D_6 detectors, are clearly evident. We used the data in Fig. 5 of Ref. [22] to estimate the effective capture areas of the fluorine and aluminum peaks to be 14.2 and 22.9 b eV, respectively. In our $^{88}\text{Sr}(n, \gamma)$ data, such peaks are not visible. However, we have used SAMMY to extract upper limits on their capture areas by fitting our data in the regions of these peaks and fixing their energies and neutron widths to the values given in Ref. [14]. The resulting upper limits from our data are 1.46 and 1.96 b eV, respectively for fluorine and aluminum. Our results must be scaled (by a factor of 1.29) to account for the larger scattering cross section of ^{208}Pb as compared to that of ^{88}Sr . The resulting ratios indicate that the sensitivity of the Geel apparatus to this background from scattered neutrons is at least 7.6 (fluorine) to 9.1 (aluminum) times worse (i.e., greater) than ours. Considering the fact that extracting an upper limit for the fluorine resonance from our data is complicated by a (much narrower) $^{88}\text{Sr}(n, \gamma)$ resonance at almost the same energy, these two ratios are in good agreement. Although the number derived from the aluminum resonance should be more reliable, we used the more conservative average ratio of 8.4. The larger neutron sensitivity of the Geel apparatus is most likely a result of the much larger amount of fluorine and aluminum in their detector housings. Because of the similarity of the apparatus, we expect that the energy dependence of this background is the same at ORELA as it is at Geel. Unfortunately, the exact energy dependence of the correction factor is not given in Ref. [22]. However, a preliminary estimate of the energy dependence of the neutron sensitivity of the Geel apparatus was given in Ref. [7]. Using the formula given in Ref. [7], we calculated a correction factor of 4.9×10^{-5} for the 77.85-keV resonance in ^{208}Pb . This value is in agreement within the quoted uncertainty with the value given (6.0×10^{-5}) for this resonance in Ref. [22]. In addition, the energy dependence of the correction factor given by the formula in Ref. [7] follows the general trend of the various estimates of the neutron sensitivity correction factor given in Ref. [22]. For these reasons, we used the energy dependence given in Ref. [7], scaled (by a factor of 6.0/4.9 to the data of Ref. [22], and scaled (by a factor of 1/8.4) for the smaller neutron sensitivity of our apparatus. The resulting upper limit on the correction for the neutron sensitivity of our apparatus, expressed as an amount by which our Γ_γ values must be reduced, is

$$C_n = 2.4 \times 10^{-4} E_r^{-0.8} \Gamma_n, \quad (8)$$

where the resonance energy, E_r , is in keV and the correction is in the same units as those of the neutron width Γ_n . This correction factor for the ORELA apparatus is compared to that for the Geel apparatus in Fig. 7.

The Γ_γ values, given in Table I, have been corrected using this formula. The corrections are negligible in almost all cases. Only 16 of the 101 resonances have corrections larger than 1%, and for eight of these the corrections are this size only because they have comparably small radiation widths ($\Gamma_\gamma < 100$ meV compared to an average Γ_γ of 200 to 300 meV). The largest correction is 7% for the 13.846-keV resonance, which has a small radiation width $\Gamma_\gamma = 80.5$ meV.

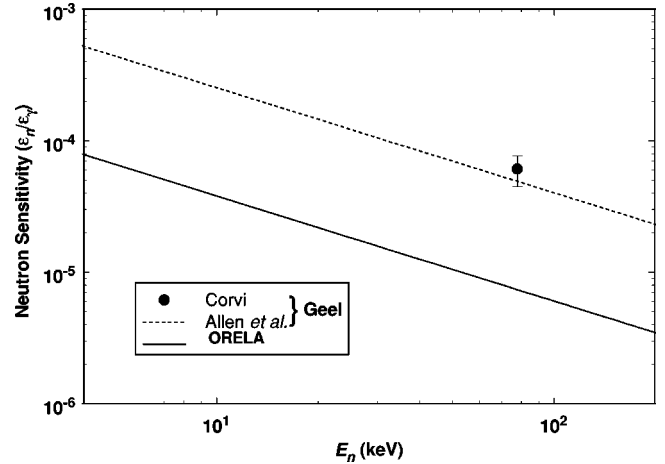


FIG. 7. Neutron sensitivity of the capture apparatus at ORELA. Plotted is the ratio of the efficiency for detecting scattered neutrons to the efficiency for detecting γ rays. The neutron sensitivity of the Geel apparatus is shown for comparison. Note that the greater the neutron sensitivity of the apparatus, the larger the sample-dependent background in the measurements. See the text for details.

Because the corrections are small and because most of the resonances with the largest corrections have relatively small capture areas or are at relatively high energies, there is very little effect on the astrophysical reaction rate determined from our data. We calculated that the effect of this correction is to decrease the reaction rate by 0.95% at $kT=8$ keV and 0.60% at $kT=30$ keV.

The smooth energy dependence of the neutron sensitivity correction indicated by Eq. (8) is only an approximation. There could be significant structure due to resonances in the materials from which the detectors and their immediate surroundings are constructed. Previous measurements (e.g., Ref. [22]) as well as Monte Carlo calculations we have made indicate that the largest effects in our apparatus should be due to aluminum and fluorine. The fact that we do not observe effects at the energies corresponding to large resonances in these materials gives us confidence that the corrections at energies away from these resonances are significantly smaller than given by Eq. (8).

V. ASTROPHYSICAL REACTION RATE

Astrophysical reaction rates, $N_A \langle \sigma v \rangle$, calculated from our data, are shown in Fig. 8. We show reaction rates rather than average cross sections to better reveal the temperature dependence apart from the $1/v$ factor. The Maxwellian-averaged cross sections $\langle \sigma \rangle = N_A \langle \sigma v \rangle / N_A v_T$ calculated from our data at selected temperatures are given in Table IV. The reaction rates and Maxwellian-averaged cross sections were calculated from our resonance parameters using the method described in Ref. [23]. In particular, the contribution from broad resonances was obtained using numerical integration. Also, the very small $1/v$ component resulting from the portion of the thermal cross section [24] (the value given in Ref. [14] is incorrect by a factor of 10) not accounted for by known s -wave resonances (in the 100 eV to 350 keV

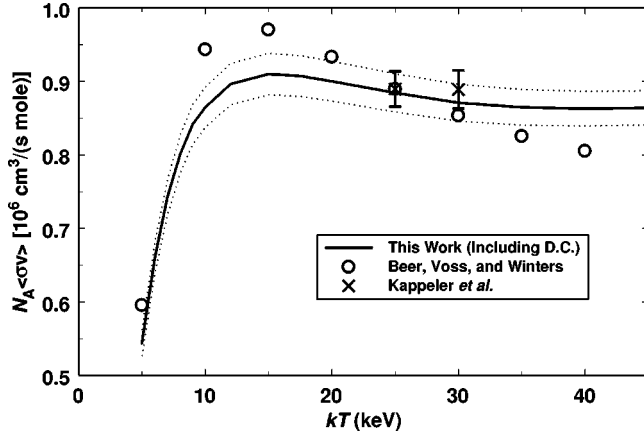


FIG. 8. Astrophysical rates for the $^{88}\text{Sr}(n, \gamma)$ reaction calculated from the data of the present work plus the calculated contribution due to direct capture (solid curve, with dashed curves depicting the uncertainties). Also shown is the evaluated rate of Ref. [23] which has been used in most previous nucleosynthesis calculations (circles) as well as the rate measured in an activation experiment [1] (\times 's).

region) was included. The statistical uncertainties in the reaction rates are negligible when compared to the overall normalization uncertainty. From the uncertainty in the $^{197}\text{Au}(n, \gamma)$ and $^6\text{Li}(n, \alpha)$ cross sections [25], the statistical precision of the calibration measurements, and the repeatability of the calibration runs, we calculate that the normalization uncertainty is 3%.

A. Direct-capture component of the reaction rate

Because the average cross section resulting from resonances is small, the contribution from direct capture (DC) of neutrons may constitute a significant portion of the total average capture cross section. This DC component cannot be measured directly using the present technique, but it can be calculated reliably because sufficient information is available from other experiments.

To determine the DC contribution to the cross section, we performed a calculation using the code TEDCA [26]. The theoretical cross section σ^{th} is derived from the direct-capture cross section σ^{DC} using [27]

$$\sigma^{\text{th}} = \sum_i C_i^2 S_i \sigma_i^{\text{DC}}. \quad (9)$$

The sum extends over all possible final states (ground state and excited states) in the final nucleus. The isospin Clebsch-Gordan coefficients and spectroscopic factors are denoted by C_i and S_i , respectively.

For the determination of the optical potentials for the bound state and the entrance channel, we used a folding procedure. In this approach the nuclear target density ρ_T is folded with an energy- and density-dependent nucleon-nucleon interaction v_{eff} [28]:

$$V(R) = \lambda V_F(R) = \lambda \int \rho_T(r) v_{\text{eff}}(E, \rho_T, |R-r|) dr, \quad (10)$$

with R being the separation of the centers of mass of the two colliding nuclei. The normalization factor λ accounts for effects of antisymmetrization and is close to unity.

The nuclear density ρ_T was calculated with the wave functions obtained from a mass model [29]. The only free parameter λ in the bound-state potential can be fixed by the requirement of reproducing the binding energy of the considered state. For the entrance channel, the value of λ was determined from elastic neutron scattering data [30]. The measured thermal scattering length was reproduced by assuming $\lambda = 0.948$. The reaction Q values were derived from the recent mass compilation [31] and experimental level information [32].

In our calculation we accounted for capture to the ground state ($5/2^+$) and to the first four excited states ($1/2^+$, $7/2^+$, $5/2^+$, $3/2^+$). The possible transitions, which are considered in the code, are $E1$, $E2$, and $M1$. The spectroscopic factors S_i were taken from a (d, p) experiment [33].

TABLE IV. Maxwellian averaged neutron capture cross sections.

| Thermal energy kT (keV) | $\langle\sigma v\rangle/v_T$ (mb) | | |
|------------------------------|-----------------------------------|---------------------------------|------------------|
| | From measurements | From direct capture calculation | Total |
| 5.0 | 8.97 | 0.22 | 9.19 ± 0.30 |
| 8.0 | 10.42 | 0.28 | 10.70 ± 0.34 |
| 10 | 10.02 | 0.31 | 10.33 ± 0.33 |
| 15 | 8.48 | 0.40 | 8.88 ± 0.27 |
| 20 | 7.13 | 0.47 | 7.60 ± 0.23 |
| 25 | 6.14 | 0.54 | 6.68 ± 0.20 |
| 30 | 5.40 | 0.61 | 6.01 ± 0.17 |
| 40 | 4.42 | 0.73 | 5.15 ± 0.16 |
| 50 | 3.81 | 0.84 | 4.65 ± 0.16 |
| 60 | 3.40 | 0.94 | 4.34 ± 0.16 |
| 70 | 3.09 | 1.02 | 4.11 ± 0.16 |
| 85 | 2.76 | 1.12 | 3.88 ± 0.16 |

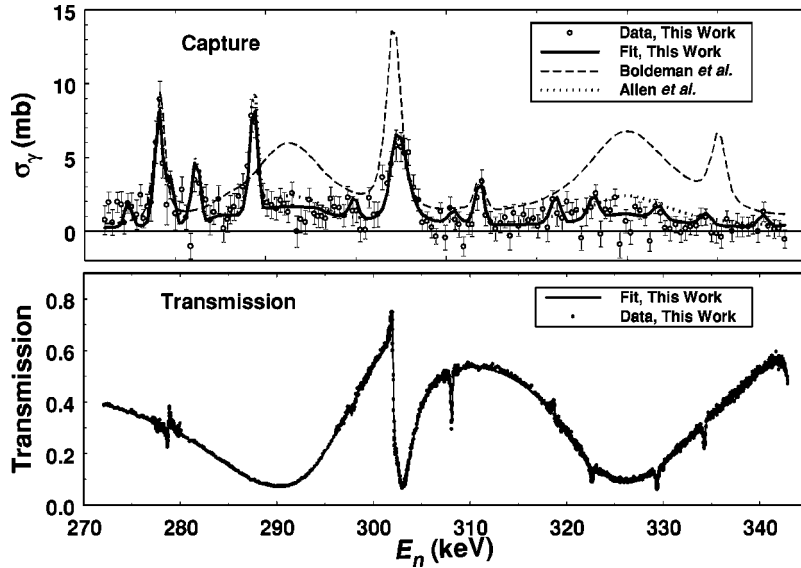


FIG. 9. ^{88}Sr neutron capture and transmission data from the present work (circles with error bars) and our SAMMY fits with the data (solid curves) in the region from 270 to 350 keV. Also shown are the effective capture cross sections calculated using the radiation widths of Refs. [5] (dotted curve) and [7] (dashed curve). See the text for details.

Because all low-lying states have positive parity, p -wave capture is dominant above thermal energy. In ^{89}Sr , negative-parity states are found only above 2.3-MeV excitation energy [32] and, therefore, will have lower Q values and small spectroscopic factors, both leading to a reduced contribution to the cross section. The negative-parity states cannot be directly included in the calculation because of the lack of spectroscopic information, but their contribution can be estimated. Assuming that the difference between the measured thermal cross section [24] and the thermal value derived from the resonance information in this work is entirely caused by s -wave direct capture, an upper limit for the DC contribution at thermal energy of about 2.2 mb can be deduced. Extrapolating the $1/v$ behavior, we arrive at an s -wave contribution of $1.9 \mu\text{b}$ at 25 keV, which is negligible.

Capture to the $1/2^+$ state at 1.032 MeV and to the $3/2^+$ state at about 2 MeV contributes most to the capture cross section because capture to states with higher spins can proceed only via odd partial waves with $l > 2$ in the case of the dominating $E1$ transition.

The total DC cross section is $\sigma^{\text{th}} = 0.33$ mb at $E_n = 25$ keV and has an energy dependence approximately proportional to $E_n^{1/2}$. Converting our result to a Maxwellian-averaged cross section, we arrive at a value of 0.54 mb at $kT = 25$ keV, as compared to 6.14 mb resulting from the measured resonances. Results at other temperatures are given in Table IV.

VI. COMPARISON TO PREVIOUS RESULTS AND DISCUSSION

Our data are compared to previous work in Figs. 8 and 9. Our results represent a substantial improvement over previous knowledge.

A. Resonance parameters

There is reasonable agreement between the capture kernels, $(g_J \Gamma_n \Gamma_\gamma / \Gamma)$, from the fits to our data and previous

work [5,7]—with the exception that the capture kernels from Ref. [5] are, on average, somewhat larger, especially for those resonances with very large Γ_n . This difference would seem to indicate that the correction for the background caused by the prompt capture of scattered neutrons was underestimated in Ref. [5]. However, there is a more obvious trend for the capture kernels of Ref. [5] to be systematically larger than ours with increasing neutron energy. It is possible that this trend could result from improper background subtraction or from improper corrections for resonance self-shielding and multiple scattering (because the neutron widths for many of the resonances were not known in the previous work) and from an undercorrection for prompt neutron background in Ref. [5]. In our work, the backgrounds were determined in separate measurements, whereas in Ref. [5] these backgrounds were estimated using a smooth function, whose magnitude was adjusted in the fitting procedure used to determine the resonance parameters. In addition, the self-shielding and multiple scattering corrections were well constrained in our work because we had transmission data. Because both the relative sizes of the backgrounds and these corrections increase with neutron energy, it is possible that the observed trend (of the capture kernels of Ref. [5] to increase with increasing neutron energy) could at least in part be due to these effects.

In Fig. 9, we see further evidence that the prompt neutron-scattering background was underestimated in Refs. [5,7]. This figure shows our capture and transmission data, our fits to these data, and the effective capture cross sections calculated using the resonance parameters of Refs. [5,7]. It is important to note that our data and our resonance parameters have *not* been corrected for the background resulting from the prompt capture of scattered neutrons, whereas the parameters of the previous works received substantial corrections for this background. The calculations using the parameters of Ref. [5] is in fairly good agreement with the data for the narrower resonances, but they are substantially larger than our capture data for the two broadest resonances near 290 and 325 keV. The calculation using the parameters of Ref.

[7] also appears to be larger than the data. However, only the parameters for the resonances with large Γ_γ were reported in Ref. [7], so our parameters were used for the other resonances which are shown in Fig. 9.

The correlation coefficients $\rho(\gamma_\lambda^2, \Gamma_{\gamma\lambda})$, which were determined from our resonance parameters, are considerably different from those of Ref. [5]. In particular, our *s*-wave correlation coefficient has opposite sign, 0.23 ± 0.06 herein vs -0.18 in Ref. [5]. In addition, our *p*-wave correlation coefficients are significantly smaller, 0.55 ± 0.09 and 0.59 ± 0.9 for $p_{1/2}$ and $p_{3/2}$, respectively, herein vs 0.78 and 0.96 in Ref. [5]. This finding is probably another indication that the neutron-sensitivity correction was underestimated in Ref. [5]. On the other hand, our *p*-wave correlation coefficients are in agreement to within the quoted uncertainties with those reported in Ref. [7], 0.40 ± 0.23 for $p_{1/2}$ and 0.57 ± 0.16 for $p_{3/2}$. Although these correlations are sizable, and our data (and analysis) are much better than those previously available, the fact that the (*lJ*) assignments for many *p*-wave resonances remain uncertain makes interpretation in terms of the valence model less than convincing. Even so, if the Γ_γ are assumed to be χ_ν^2 distributed, then the variances of the observed distributions suggest $\nu=3$ and $\nu=7$ for the $p_{1/2}$ and $p_{3/2}$ resonances, respectively. The small number of radiation partial widths these numbers imply is also consistent with the valence model.

The average radiation width for the firm *s*-wave resonances we observed (190 meV) is in reasonable agreement with the value reported (220 meV) in Ref. [5]. On the other hand, the values we measure for the average $p_{1/2}$ (220 meV) and $p_{3/2}$ (280 meV) radiation widths are more than a factor of 2 smaller than those reported (both 670 meV) in Ref. [5]. Because in the present case *p*-wave resonances tend to be much broader than *s*-wave resonances, it is likely that the much larger average radiation widths for *p*-wave resonances reported in Ref. [5] were the result of an undercorrection for the backgrounds and self-shielding effects which are discussed previously.

The values of the conventionally defined *s*- and *p*-wave strength functions calculated from our resonance parameters (0.32 ± 0.06 and 5.1 ± 0.6 , respectively, in units of 10^{-4}) are consistent with those resulting from earlier work (0.45 ± 0.1 , 5.0 ± 0.7) [14]. Similarly, our value for the *s*-wave potential scattering radius (6.8 fm) is in agreement with earlier work (7.1 fm) [14].

B. Reaction rates

There is no indication of the resonance reported in Ref. [8] at 2.780 keV in our capture or transmission data on ^{88}Sr ; hence, if this resonance exists, it is much too small to have any significant impact on the astrophysical reaction rate. The most likely explanation seems to be that this resonance is actually in another strontium isotope. In Ref. [14], there is a resonance reported in $^{87}\text{Sr}+n$ at very nearly the same energy (2.756 keV). In addition, (*n, γ*) measurements that we have made with a natural strontium sample also show a resonance at this energy.

The reaction rate determined in this work is compared to previous results [1,23] in Fig. 8. For Ref. [1], we show the result of the actual measurement at $kT=25$ keV in addition to the more commonly quoted value resulting from the extrapolation to $kT=30$ keV. We do so because the $1/\nu$ shape, used in Ref. [1] for this extrapolation, is clearly incorrect, as shown in Fig. 8. Our total (resonance plus direct capture) reaction rate at $kT=25$ keV is in excellent agreement with the activation measurement of Ref. [1]. This result lends further confidence to our direct-capture calculation because the difference between the Maxwellian-averaged cross section determined from our resonance data alone and the activation measurement of Ref. [1] (0.58 ± 0.27 mb), is in excellent agreement with the calculated direct contribution (0.54 mb). Hence, for the first time with our new data, the $^{88}\text{Sr}(n, \gamma)$ reaction rate is known with good precision across the entire range of temperatures needed by stellar models of the *s* process.

The evaluated rate of Ref. [23] has been used most frequently in recent *s*-process nucleosynthesis calculations. Unfortunately, the authors of Ref. [23] used the resonance parameters given in Ref. [14] rather than those in the primary sources to calculate the reaction rate. In Ref. [14], the radiation width of the first *s*-wave resonance at 13.852 keV was scaled upward by 35% to fit the thermal cross section. Because the level density is fairly low and because this resonance is rather broad, this change causes a significant increase in the reaction rate across a range of temperatures, as compared to the rate calculated using the reported [5] radiation width for this resonance. It is also important to note that both the rate and its uncertainty given in Ref. [23] have been scaled [34] to the single-temperature measurement of Ref. [1]; hence, the uncertainty given in Ref. [23] is too small, except at $kT=25$ keV. Moreover, subsequent correction factors [35] to the data of Ref. [5] have been disregarded in Ref. [23].

Even with the addition of the calculated direct-capture component, our new rate is still about 9.5% smaller than that of Ref. [23] in the $kT=6-8$ keV region, where most of the neutron exposure occurs in current *s*-process stellar models. This smaller reaction rate will, in general, lead to an increase in the ^{88}Sr abundance calculated by a given *s*-process model or, alternatively, to a lower neutron exposure required in the model to reproduce the observed abundances. With our new rate, the agreement between the results of stellar *s*-process model calculations [36] and recently measured isotopic ratios in meteoric SiC grains [3] has improved although significant differences remain. For example, the calculated $^{88}\text{Sr}/^{86}\text{Sr}$ ratios show a much wider variation than the measured ratios, and, when plotted versus $^{84}\text{Sr}/^{86}\text{Sr}$, appear to be systematically smaller than the measured ratios over most of the range of $^{84}\text{Sr}/^{86}\text{Sr}$. These differences may be providing important clues for improving stellar models of the *s* process. However, the relatively large uncertainties in the $^{86,87}\text{Sr}(n, \gamma)$ reaction rates cloud the comparison between theory and experiment; so, more precise measurements for these rates are needed to attempt to understand these differences in terms of stellar models.

ACKNOWLEDGMENTS

This research was supported by the U.S. Department of Energy under Contract No. DE-AC05-00OR22725 with UT-Battelle, LLC and Contract No. DE-FG02-87ER40326 with Denison University, and by the U.S. National Science Foun-

dation under Contract No. NSF-AST-97-31569 with the University of California at Santa Cruz. R.R.W. was supported in part by the Joint Institute for Heavy Ion Research. T.R. was supported by the Swiss National Science Foundation under Grant No. 2124-055832.98.

-
- [1] F. Käppeler, W. R. Zhao, H. Beer, and U. Ratzel, *Astrophys. J.* **355**, 348 (1990).
- [2] D. L. Lambert, V. V. Smith, M. Busso, R. Gallino, and O. Straniero, *Astrophys. J.* **450**, 302 (1995).
- [3] G. K. Nicolussi, M. J. Pellin, R. S. Lewis, A. M. Davis, R. N. Clayton, and S. Amari, *Phys. Rev. Lett.* **81**, 3583 (1998).
- [4] R. L. Macklin and J. H. Gibbons, *Astrophys. J.* **149**, 577 (1967).
- [5] J. W. Boldeman, B. J. Allen, A. R. D. L. Musgrove, R. L. Macklin, and R. R. Winters, *Nucl. Phys.* **A269**, 397 (1976).
- [6] F. Käppeler, R. Gallino, M. Busso, G. Picchio, and C. M. Raiteri, *Astrophys. J.* **354**, 630 (1990).
- [7] B. J. Allen, R. Shelley, T. V. der Veen, A. Brusegan, and G. Vanpraet, in *Capture Gamma-ray Spectroscopy and Related Topics*, edited by T. V. Egidy, F. Gonnenswein, and B. Maier (IOP, Bristol, 1981), p. 404.
- [8] Y. V. Adamchuck, L. S. Danelyan, S. S. Moskalev, G. V. Muradyan, and Y. G. Shchepkin, *Euronuclear* **2**, 183 (1965).
- [9] R. L. Macklin, J. Halperin, and R. R. Winters, *Nucl. Instrum. Methods* **164**, 213 (1979).
- [10] P. E. Koehler, R. R. Spencer, R. R. Winters, K. H. Guber, J. A. Harvey, N. W. Hill, and M. S. Smith, *Phys. Rev. C* **54**, 1463 (1996).
- [11] R. L. Macklin and B. J. Allen, *Nucl. Instrum. Methods* **91**, 565 (1971).
- [12] N. M. Larson, Technical Report No. ORNL/TM-9179/R3, Oak Ridge National Laboratory, 1996 (unpublished).
- [13] P. E. Koehler, R. R. Spencer, K. H. Guber, J. A. Harvey, T. Rauscher, J. C. Blackmon, S. Raman, D. C. Larson, D. W. Bardayan, and T. A. Lewis, in *Nuclei in the Cosmos*, edited by N. Prantzos and S. Harissopulos (Editions Frontières, Paris, 1998), p. 196.
- [14] S. F. Mughabghab, M. Divadeenam, and N. E. Holden, *Neutron Cross Sections* (Academic, New York, 1981), Vol. 1.
- [15] C. E. Porter and R. G. Thomas, *Phys. Rev.* **104**, 483 (1956).
- [16] M. S. Moore, J. D. Moses, and G. A. Keyworth, *Phys. Rev. C* **18**, 1328 (1978).
- [17] R. R. Winters, R. F. Carlton, C. H. Johnson, N. W. Hill, and M. R. Lacerna, *Phys. Rev. C* **43**, 492 (1991).
- [18] F. J. Dyson and M. L. Metha, *J. Math. Phys.* **4**, 489 (1963).
- [19] A. M. Lane and J. E. Lynn, *Nucl. Phys.* **17**, 586 (1960).
- [20] R. F. Carlton, R. R. Winters, C. H. Johnson, N. W. Hill, and J. A. Harvey, *Phys. Rev. C* **38**, 1605 (1988).
- [21] C. H. Johnson and R. R. Winters, *Phys. Rev. C* **21**, 2190 (1980).
- [22] F. Corvi, in *Proceedings of the Specialists Meeting on the Measurement, Calculation, and Evaluation of Photon Production Data*, edited by C. Coceva (NEA, Bologna, 1995), No. NEA/NSC/DOC(95)1, p. 229.
- [23] H. Beer, F. Voss, and R. R. Winters, *Astrophys. J., Suppl. Ser.* **80**, 403 (1992).
- [24] J. C. Roy, P. J. Berry, and L. P. Roy, *Can. J. Chem.* **36**, 731 (1958).
- [25] H. Beer and R. L. Macklin, *Phys. Rev. C* **26**, 1404 (1982).
- [26] H. Krauss (unpublished).
- [27] K. H. Kim, M. H. Park, and B. T. Kim, *Phys. Rev. C* **23**, 363 (1987).
- [28] A. M. Kobos, B. A. Brown, R. Lindsay, and G. R. Satchler, *Nucl. Phys.* **A425**, 205 (1984).
- [29] E. R. Hilf, H. V. Groote, and K. Takahashi, *Proceedings of the Third International Conference on Nuclei Far from Stability* (CERN 76-13, Geneva, 1976), No. CERN 76-13, p. 142.
- [30] L. Koester, K. Knopf, and W. Waschkowski, *Z. Phys. A* **301**, 215 (1981).
- [31] G. Audi and A. H. Wapstra, *Nucl. Phys.* **A595**, 409 (1995).
- [32] R. B. Firestone, *Table of Isotopes*, 8th ed. (Wiley, New York, 1996).
- [33] C. Winter, B. Krusche, K. P. Lieb, S. Michaelsen, G. Hlawatsch, H. Linder, T. V. Egidy, F. Hoyler, and R. F. Casten, *Nucl. Phys.* **A491**, 395 (1989).
- [34] H. Beer (private communication).
- [35] B. J. Allen, J. W. Boldeman, and R. L. Macklin, *Nucl. Sci. Eng.* **82**, 230 (1982).
- [36] R. Gallino (private communication).